ASOs are an effective treatment for disease-associated oligodendrocyte signatures in premanifest and symptomatic SCA3 mice

Kristen H. Schuster[1], Annie J. Zalon[1], Danielle M. DiFranco[1], Alexandra F. Putka[1,2], Nicholas Stec[1], Sabrina Jarrah[1], Arsal Naeem[1], Zaid Haque[1], Hongjiu Zhang[3], Yuanfang Guan[3], and Hayley S. McLoughlin[1]

[1]Department of Neurology, University of Michigan, Ann Arbor, MI 48109
[2]Neuroscience Graduate Program, University of Michigan, Ann Arbor, MI 48109
[3]Department of Computational Medicine and Bioinformatics, University of Michigan, Ann Arbor, MI 48109

Address correspondence to:
Hayley McLoughlin
4013 BSRB, 109 Zina Pitcher Pl.
Ann Arbor, MI 48109
hayleymc@med.umich.edu

SHORT TITLE: ASOs treat SCA3 oligodendrocyte maturation impairments

KEYWORDS
Ataxia, antisense oligonucleotide, oligodendrocyte, myelination, Machado-Joseph disease, Spinocerebellar ataxia type 3, polyglutamine

ABSTRACT

Spinocerebellar ataxia type 3 (SCA3) is the most common dominantly inherited ataxia. Currently, no preventative or disease-modifying treatments exist for this progressive neurodegenerative disorder, although efforts using gene silencing approaches are under clinical trial investigation. The disease is caused by a CAG repeat expansion in the mutant gene, *ATXN3*, which produces an abnormally enlarged polyglutamine tract in the mutant ATXN3 protein. Similar to other paradigmatic neurodegenerative diseases, studies evaluating the pathogenic mechanism focus primarily on neuronal implications. Consequently, therapeutic interventions generated to target these deficiencies often overlook non-neuronal contributions to disease. Our lab recently reported that oligodendrocytes display some of the earliest and most progressive dysfunction in SCA3 mice. Evidence of disease-associated oligodendrocyte signatures has also been reported in other neurodegenerative diseases, including Alzheimer's disease, ALS, Parkinson's disease, and Huntington's disease. Here, we assess the effects of anti-*ATXN3* antisense oligonucleotide (ASO) treatment on oligodendrocyte dysfunction in both premanifest and symptomatic SCA3 mouse models. We report a severe, but modifiable, deficit in oligodendrocyte maturation caused by the toxic gain-of-function of mutant ATXN3 early in SCA3 disease progression that is transcriptionally, biochemically, and functionally rescued with anti-*ATXN3* ASO. Our results establish the necessity of considering non-neuronal targets in future neurodegenerative disease therapies.

INTRODUCTION

Spinocerebellar ataxia type 3 (SCA3), also known as Machado-Joseph disease, is the most common dominantly inherited ataxia in the world[1]. It is caused by a CAG trinucleotide repeat expansion in exon 10 of the *ATXN3* gene, which translates to an expanded polyglutamine (polyQ) repeat in the ATXN3 protein. SCA3 patients experience progressive loss of motor control[2-4] with neuronal death and gliosis in specific regions of the brain, including the deep cerebellar nuclei (DCN), pontine nuclei, and spinocerebellar tract[5-7]. To date, no treatments exist for this uniformly fatal disorder. Current research focusing on identifying targets for therapeutic intervention has demonstrated gene suppression to be a promising strategy, as silencing of *ATXN3* is well-tolerated in mouse models of SCA3[8-11].

Of the available gene suppression methods, antisense oligonucleotides (ASOs) are a powerful, non-viral tool for the treatment of neurological disorders. ASOs involve a single-strand oligonucleotide binding a complimentary target mRNA to prevent translation. Numerous preclinical and clinical trials are ongoing that aim to assess ASO efficacy for the treatment of neurodegenerative diseases that have historically lacked viable therapeutic options[12-16]. Toward SCA3 disease, previous proof-of-concept studies established the safety and efficacy of ASOs as a disease-modifying therapy in SCA3 mouse models[9,10,17-20]. Our group has demonstrated widespread distribution of an anti-*ATXN3* ASO (hereafter referred to as ASO-5) throughout the central nervous system (CNS) after intracerebroventricular (ICV) injection of an 8-week-old symptomatic mouse[9]. ASO-5 effectively targeted SCA3-relevant neuronal populations in areas of the brain that are particularly vulnerable to degeneration, including pontine and deep cerebellar nuclei[9,18]. Nuclear accumulation of ATXN3 decreased, as did oligomeric high molecular weight ATXN3 expression levels. Further, sustained ASO-5 treatment significantly improved motor dysfunction in homozygous SCA3 mice (Q84/Q84 mice), although there was no rescue of mouse weight[18]. In sum, our lab has demonstrated ASO-mediated ATXN3 suppression as an effective and well-tolerated approach to reduce human mutant ATXN3 levels throughout the brain and rescue locomotor activity in symptomatic mice. This work provides the proof-of-concept framework for evaluating

the efficacy of anti-*ATXN3* ASO in SCA3 patients, which is ongoing (ClinicalTrials.gov Identifier: NCT05160558).

Although ASOs have been shown to be a compelling treatment strategy in SCA3, an outstanding gap in this field is the effect of ASOs on non-neuronal cells. Most research investigating the mechanisms contributing to neurodegeneration in SCA3 has focused on neuronal dysfunction. Our lab recently established that among the earliest and most progressive changes in SCA3 disease is an oligodendrocyte (OL) maturation defect[21]. Through RNA sequencing (RNAseq) analysis, we identified robust differentially expressed genes implicating OL dysfunction in disease pathogenesis. With transcriptional, biochemical, and histological verification, we confirmed impairments in OL maturation that corresponded to abnormal myelination in SCA3 mice. We further confirmed in SCA3 post-mortem cerebellar tissue significant white matter loss by histology and biochemical analysis[22]. Similar disease-associated oligodendrocyte signatures have been reported in other neurodegenerative diseases, including Alzheimer's disease, Amyotrophic Lateral Sclerosis (ALS), Parkinson's disease, and Huntington's disease[23-26]. Many of these neurodegenerative disease programs also have preclinical and clinical development of ASO therapy[12-16]. Therefore, in this study we utilized SCA3 mice as a paradigmatic model of OL dysfunction in neurodegenerative diseases to test the efficacy of ASO treatment on SCA3 OL maturation impairments.

We first addressed if we could prevent OL maturation impairments by treating SCA3 mice with ASO-5 prior to motor dysfunction. We show the impact of premanifest suppression of *ATXN3* on secondary phenotypes, such as motor activity and mouse weight, as well as the prevention of OL transcriptional impairments across three vulnerable brain regions: the brainstem, cerebellum, and spinal cord. Because the majority of ASO treatments are being evaluated in early symptomatic patients, we then assessed if treatment of ASO-5 in symptomatic SCA3 mice alleviates OL dysfunction. Through transcriptional profiling of treated mice brain tissue, we show rescue of gene expression and gene ontology terms important for OL maturation. We further confirmed temporal rescue of these OL impairments across vulnerable SCA3 brain regions by biochemical and histological assessments. We validated ASO rescue of myelination by TEM analysis of a vulnerable brain region in SCA3, the corticospinal tract. By evaluating

premanifest and symptomatic injection of an anti-*ATXN3* ASO, we determine the efficacy of ASO-5 treatment on OL maturation defects and validate the importance of considering non-neuronal disease contributions in future therapeutic interventions.

RESULTS

PRE-SYMPTOMATIC ANTI-ATXN3 ASO DELIVERY PREVENTS LOCOMOTOR AND WEIGHT PHENOTYPES IN SCA3 MICE

SCA3 is believed to primarily be caused by the gain-of-toxic-function of mutant ATXN3. Because of this, we first sought to determine whether knocking down *ATXN3* prior to dysfunction would hinder OL transcriptional impairments. We previously reported dysregulation of OL transcripts begins between 3 and 4 weeks of age in homozygous Q84 mice[21]. Interestingly, this immediately follows the end of the highest rate of myelination in mice, which occurs between post-natal day 7 and 21[27]. To ensure delivery of ASO-5 therapy before OLs begin to mature, we treated post-natal day 0 mice via stereotactic ICV injection with 20 µg of ASO-5 (**Fig 1A**). Weights were recorded weekly for 4 weeks, after which locomotor activity was assessed and tissue was collected (**Fig 1B**). The reduced weight typically seen in disease mice relative to wildtype littermates at 4 weeks old was not evident in either male or female disease mice treated with ASO-5 (**Fig 1C**). This is important to note, as our previously reported ASO treatment in adult-aged symptomatic mice did not have any restorative effect on weight[18]. Further, motor impairments at 4 weeks of age in Q84 vehicle treated mice were prevented with ASO-5 treatment (**Fig 1D-E**). ASO-5 treated disease mice were indistinguishable from wildtype littermates on both total locomotor activity and rearing behavior assessments (**Fig 1D-E**)**.** As this is the first study to evaluate ASO treatment in neonate SCA3 mice, we established the spread of ASO expression throughout the brain. Utilizing an anti-ASO antibody, we verified consistent ASO expression confined within the brain with no spread to peripheral tissues (**Fig 1F**). These data suggest early treatment to silence mutant *ATXN3* may be an effective strategy in delaying or preventing the onset of SCA3, highlighting the importance of identifying quantifiable biomarkers early in disease.

PREMANIFEST ASO-5 TREATMENT SUPPRESSES MUTANT ATXN3 AND PREVENTS TRANSCRIPTIONAL OLIGODENDROCYTE MATURATION IMPAIRMENTS IN VULNERABLE SCA3 BRAIN REGIONS

To confirm ASO-5 treatment in post-natal day 0 mice targets and silences *ATXN3* expression, we transcriptionally analyzed three of the most vulnerable brain regions in SCA3, the brainstem, cerebellum, and spinal cord at 4 weeks of age. We found that ASO-5 treatment in disease mice decreases expression of both the human and mouse *ATXN3* transcript from brainstem and spinal cord tissue relative to vehicle-treated disease mice (**Fig 2A-B**). Cerebellum tissue showed no significant differences in ASO ATXN3 gene silencing (**Fig 2A-B**), possibly indicating reduced targeting to this region by neonate ICV injection or a faster turnover of ASO in the area 4 weeks after treatment. While the monomeric mutant ATXN3 (mutATXN3) protein was not significantly decreased in any brain region assessed 4 weeks after treatment (**Fig 2C-D**), the high molecular weight (HMW) ATXN3 protein was significantly reduced in all tissue samples (**Fig 2C, E**).

Dysregulation in mature myelinating OL transcripts begins between 3 and 4 weeks of age in Q84 mice[21], therefore we addressed if the onset of this impairment could be impeded with premanifest ASO treatment. Indeed, in the brainstem, cerebellum, and spinal cord, many of the representative OL maturation transcripts were expressed at levels comparable to WT levels through 4 weeks of age (**Fig 2F-I**). Our previous study showed that changes in mature OL RNA expression translated to reduced mature OL protein expression[21], though not until 8 weeks of age in Q84 mice. Due to the study design, we are unable to evaluate the downstream translational effects at 4 weeks. However, RNA recovery indicates that even in a premanifest state, these OL transcripts are relevant and modifiable. Further, these results suggest the onset of this oligodendrocyte-associate disease signature could be delayed with early treatment.

ASO-5 TREATMENT OF A SYMPTOMATIC SCA3 MOUSE REDUCES ATXN3 AND RESCUES DISEASE-ASSOCIATED OLIGODENDROCYTE SIGNATURES

Previous studies from our lab established successful ASO-mediated ATXN3 suppression and behavioral rescue in the same mouse model with treatment after

symptomatic onset[18]. Therefore, we next sought to evaluate if OL maturation impairments were also rescued in treated symptomatic SCA3 mice. As several disease phenotypes, including behavior, histopathology, and OL maturation impairments, are evident by 8 weeks of age in SCA3 mice[18,21,28,29], this age was defined as 'symptomatic'. We treated 8-week-old Q84 mice with ICV injection of ASO-5 or vehicle and compared to vehicle-treated WT littermates (**Fig 3A**). Because phenotypic rescue after ASO treatment has been shown to persist for up to 8 weeks[18], we harvested brain tissue from mice at 16 weeks of age. We extracted RNA from two of the most vulnerable brain regions in SCA3, the brainstem and cerebellum (**Fig 3A**) and transcriptionally profiled these regions from each treatment group via RNAseq. All tissue samples assessed by paired end RNAseq had an RNA integrity number (RIN) greater than seven. The average number of read counts per brainstem sample was 50.5 million (SD ± 7.5 million), with an average of 83.4% of sequencing reads mapping to exons of known genes. The average number of read counts per cerebellum sample was 31.0 million (SD ± 2.7 million), with an average of 82.1% of sequencing reads mapping to exons of known genes.

RNAseq analysis confirmed suppression of human *ATXN3* gene expression in ASO treated disease mice relative to their vehicle treated counterparts in the brainstem, but only trending reduction in the cerebellum (**Fig 3B, F**). We validated transcript knockdown with protein analysis via Western blot and found that compared to vehicle treatment, ASO-5 treatment in disease mice partially reduced both aggregated (HMW) and monomeric (mutATXN3) disease-associated ATXN3 in brainstem, but only mutATXN3 in the cerebellum (**Fig 3C-E, G-I**). Bioinformatic analysis of differentially expressed (DE) gene expression ($q<0.05$) between WT and Q84 vehicle treated mice showed 750 and 39 DE genes in the brainstem and cerebellum, respectively (**Fig 3J**). In brainstem tissue, ASO-5 treatment resulted in only 9 DE genes relative to WT vehicle treated, whereas 51 DE genes were noted between ASO-5 and vehicle treated disease tissue (**Fig 3J, top**). In the cerebellar RNAseq analysis, there were 38 DE genes between ASO-5 treated disease tissue relative to WT vehicle treated tissue and 12 genes DE between ASO-5 and vehicle treated disease mice (**Fig 3J, bottom**). Because limited DE genes were found in cerebellar samples, we assessed gene ontology (GO)

from only brainstem RNAseq data and found the top biological processes disrupted in SCA3 diseased mice compared to vehicle injected WT controls involve cholesterol synthesis and monocyte regulation (**Fig 3K**). Interestingly, top processes changed with ASO treatment in Q84 mice are predominantly related to myelination and OL differentiation (**Fig 3L**). Thus, GO term analysis offers insight into potential mechanisms of SCA3 ASO-5 therapy that warranted further investigation.

MYELINATION PATHWAY TRANSCRIPTS AND PROTEIN ARE RESCUED WITH ASO-5 TREATMENT IN SCA3 VULNERABLE BRAIN REGIONS

To determine how GO term myelination pathways in treated and nontreated symptomatic mice are affected throughout the mouse brain, we transcriptionally analyzed representative OL maturation genes in three of the most affected brain regions in SCA3, the brainstem (BS) (**Fig 4A**), cerebellum (CB) (**Fig 4B**), and spinal cord (SC) (**Fig 4C**). In the brainstem and spinal cord, a marker for OPCs (*Smoc1*) was found to be increased in disease, whereas markers for differentiating (*Plp1* and *Ugt8a*) and mature OLs (*Mobp* and *Mal*) in all three brain regions were decreased in disease relative to WT (**Fig 4A-C**). Consistent with premanifest treatment, symptomatic ASO-5 therapy was effective at restoring, at least partially, regional OL maturation transcripts to WT levels across all tissue samples (**Fig 4A-C**). We then assess protein changes by western blotting for MOBP, a protein expressed only in mature myelinating OLs. In the brainstem and spinal cord, mature OL protein changes matched mature OL transcript changes in that total MOBP protein levels were decreased in disease mice and rescued to WT levels with ASO-5 treatment (**Fig 4D, F**). MOBP protein levels in the cerebellum mirrored these trends, though not significantly **(Fig 4E)**. It is important to note that in SCA3, the most vulnerable part of the cerebellum is located in the deep cerebellar nuclei (DCN), which comprises only a small part of the cerebellum. Therefore, although total MOBP protein levels in the cerebellum were not significantly changed, reduction and rescue of mature OL protein may be diluted by whole cerebellum analysis. This data, combined with RNAseq GO term analysis (**Fig 3K-L**) confirms that effective therapeutic interventions for SCA3 will likely need to target OLs and myelination pathways in order to improve disease phenotypes.

To understand the cellular implications of regional OL transcript and protein expression rescue, we examined mature OL cell counts utilizing the BAC transgenic *Mobp*-eGFP reporter mouse[30] crossed with SCA3 mice. We previously used this mouse model cross to show that in SCA3 vulnerable brain regions (pons and DCN), mature *Mobp*-eGFP positive OLs are significantly reduced in a dose-dependent disease manner[21]. Thus, we questioned if mature OL cell counts could be rescued with ASO-5 treatment at a timepoint in which behavior is also rescued[18]. To determine if mature OL cell counts return to WT levels post-ASO-5 injection, we treated 8-week-old SCA3;*Mobp*-eGFP mice with 700 µg of ASO-5 and histologically evaluated the pons and DCN at 12 weeks of age. In both brain regions, we observed a reduction of mature OLs in vehicle treated disease mice compared to vehicle treated WT mice, with ASO-5 treatment rescuing *Mobp*-eGFP+ cell counts in Q84 mice (**Fig 4G-H**). Overall, these results demonstrate the efficacy of anti-*ATXN3* ASO in rescuing OL maturation impairments at the transcriptional, biochemical, and cellular level in symptomatic SCA3 mice.

ASO-5 TREATMENT ACTIVATES MYELINATION IN BOTH VULNERABLE AND NON-VULNERABLE SCA3 BRAIN REGIONS

We previously defined the reduction of mature OLs to correspond to ultrastructural abnormalities of the myelin sheath in the corticospinal tract (CST), a SCA3 vulnerable brain region[21,31]. Accordingly, in this study we investigated whether transcriptional, biochemical, and histological OL rescue is confirmed at the ultrastructural level. At 8-weeks-old, control Q84 and WT mice were treated with vehicle, while treatment group Q84 mice were treated with ASO-5. Tissue was collected and fixed 8 weeks later for TEM analysis of g-ratio and axon caliber at 16 weeks of age. Consistent with previous data, axon caliber was unchanged between vehicle treated groups and g-ratio was increased, signifying thinner myelination in Q84 controls compared to WT controls, (**Fig 5A, C-D**), whereas ASO-5 treatment in Q84 mice completely rescued myelination, as indicated by g-ratio (**Fig 5A, C**). ASO-5 treatment also led to an increased axon diameter in the CST relative to vehicle treated mice (**Fig 5A, D**). Importantly, the percentage of degenerated axons is not significantly different

between treatment groups in this region **(Fig 5B**)**,** suggesting that neither the impairment nor the rescue of OL maturation is due to exogenous neuronal signaling. Comparison of g-ratio to axonal caliber shows that larger axons in SCA3 vehicle treated mice have thinner myelination relative to WT vehicle treated mice, and that ASO-5 treatment also rescues this phenotype (**Fig 5E**).

Because ASO treatment is broadly distributed throughout the brain, we were able to explore the effects of ASO treatment on less vulnerable brain regions. The corpus callosum (CC) is a prominent white matter tract that we found to not have OL maturation impairments, as defined by mature OL cell counts, at 16 weeks old in SCA3 mice[21]. Therefore, we assessed regional OL maturation dysfunction by analyzing the ultrastructural features of myelination in this non-vulnerable brain region in vehicle and ASO-treated SCA3 mice (**Fig 5F**). As expected, we found no differences between WT and Q84 vehicle treated mice in myelination in the CC (**Fig 5G**). However, unlike ASO treatment in the CST, axon caliber in the CC was not changed in any of the conditions assessed (**Fig 5H**). ASO treatment in SCA3 mice did not further increase the axon caliber in the CC, however it did lead to substantial increases in myelination thickness as defined by the g-ratio (**Fig 5G**), particularly in smaller sized axons (**Fig 5I**). This suggests there may be a positive-reinforcement mechanism regulating myelination that garners further mechanistic exploration. These data illustrate the complete ultrastructural rescue of OLs in SCA3 and highlight the importance of considering the effects of broad-target therapies in less-affected brain regions in disease.

DISCUSSION

Previous work from our lab established an impairment in the OL maturation process as an early and progressive feature of SCA3 pathogenesis. Disease-associated oligodendrocyte signatures have also recently been attributed in more common neurodegenerative diseases like Alzheimer’s disease, Parkinson’s disease, ALS, and Huntington’s disease[23-26]. Many of these neurodegenerative disease programs also have preclinical and clinical development of ASO therapy that have yet to assess rescue of oligodendrocyte signatures[12-16]. Therefore, we tested the efficacy of ASO treatment in SCA3 mice as a paradigmatic model of OL dysfunction in

neurodegenerative diseases. The aim of the present study was to determine if anti-*ATXN3* ASO therapy can effectively treat OLs to prevent or rescue the maturation defect in SCA3. We demonstrate the therapeutic effects of ASO treatment on OL maturation dysregulation at two timepoints, premanifest and symptomatic. We provide evidence that ASO-5 treatment prior to symptom onset not only precludes OL transcript and protein dysregulation, but also prevents secondary phenotypes such as motor defects and weight loss. This suggests early treatment could be protective against SCA3 symptomatic onset. Importantly, symptomatic treatment rescued OL transcriptional dysregulation in SCA3 vulnerable brain regions, which translated to both protein and ultrastructural rescue. These results highlight the importance of considering the role of OLs in disease progression and as targets in future neurodegenerative disease therapies.

ASOs are known to broadly target all cell types of the brain– neurons and glia alike[32-35]. However, analysis of GO biological processes within brainstem tissue of ASO-5 treated Q84 mice relative to vehicle treated Q84 mice indicated heavy involvement of OLs over all other cell types: ensheathment of neurons and axons, myelination, glial cell differentiation, and organic hydroxy compound biosynthesis. OL involvement in the top four pathways is clear, however the relevance of hydroxy compound biosynthesis is not as obvious. Hydroxy compounds are essential for making cholesterol, which in turn is a primary component of myelin sheaths[36,37]. Our findings suggest that ASO-5 confers a therapeutic effect partially by influencing pathways related to OLs, indicating that OLs could be a crucial therapeutic target in SCA3. Highlighting this, a recent study in drosophila showed that expression of hyperexpanded polyQ tracts in ATXN3 only in glia resulted in developmental lethality[38]. Future investigations will need to explore the necessity and sufficiency of both the expression and silencing of mutant ATXN3 in OLs for SCA3 pathogenesis and treatment.

A key feature among many of these neurodegenerative diseases is regional vulnerability. As we previously showed[21] and extend here, OL maturation impairments are central to the regional vulnerable nervous system pathogenesis in SCA3. The brainstem and cerebellum have been established as two of the most vulnerable brain regions in SCA3 in both patients and animal models. In agreement with recent SCA3

patient literature, our findings indicate the spinal cord is also a vulnerable brain region in SCA3 mice. Although there is little SCA3 research on animal spinal cord tissue, we found it to be as affected as the brainstem, another myelin-rich white matter brain region. Interestingly, while many white matter tracts are affected in SCA3, the CC remained unaffected. We have previously shown that this region has no change in mature OL cell counts[21] and use this study to further establish the CC as a non-vulnerable brain region in SCA3 with ultrastructural analysis via TEM. Although we found no differences in myelin thickness between vehicle treated groups, ASO-5 treatment, that rescued myelination in a vulnerable brain region, surprisingly led to hypermyelination in the CC. Instead of regional vulnerability, these findings point to the possibility of regional *protection*. Much of the current work on SCA3 focuses on what causes dysfunction in vulnerable brain regions. With this study we shift the viewpoint, indicating that just as relevant will be investigations of what *prevents* dysfunction in non-vulnerable, or protected, brain regions.

This study emphasizes the importance of considering non-neuronal contributions to disease when evaluating therapeutic interventions. OLs in particular have emerged as a key player in not only SCA3 pathogenesis, but in several other neurodegenerative diseases as well, and here, we establish their therapeutic relevance. While ASOs continue to be powerful tool for SCA3 treatment, future studies into their role in rescuing dysregulated processes and possibly over-activating protective processes, in addition to their mechanism of targeting OLs, will be essential. These mechanistic studies will offer insight into the pathophysiology and therapeutic options for SCA3, as well as other neurodegenerative diseases that have disease-associated oligodendrocyte signatures.

MATERIALS AND METHODS

Animals

The University of Michigan Institutional Animal Care and Use Committee (IACUC) approved all animal procedures. They were conducted in accordance with the U.S. Public Health Service's Policy on Human Care and Use of Laboratory Animals. All animals were housed in a room following standard 12-hour light/dark cycles. Food and water were available at all times.

In this study, homozygous YACMJD84.2Q-C57BL/6 transgenic mice (referred to in this study as “Q84 mice”) and wild type (WT) sex- and age-matched controls were used. Genotyping was completed via tail biopsy DNA isolation prior to weaning and confirmed postmortem. The number of CAG repeats in the human *ATXN3* gene in Q84 mouse DNA was determined by fragmentation analysis (Laragen, San Diego, CA) as previously described[21] with all enrolled mice having a minimum CAG repeat average greater than 75. Genotyping for *Mobp*-eGFP mice was completed as previously described[21]. For all studies, 4-6 mice (equal numbers of males and females) per genotype were collected for tissue analysis at 4, 12, or 16 weeks of age. Left hemisphere brain tissue was macrodissected into brainstem (includes whole of brainstem, stratum, and thalamus), cerebellum, and cervical spinal cord for biochemical analysis as previously described[9]. PBS perfused right hemispheres were post-fixed in 4% paraformaldehyde and embedded in 30% sucrose.

Antisense Oligonucleotides

ASO-5 used in this study targets the human and mouse ATXN3 3’-UTR (ASO-5; GCATCTTTTCATTACTGGC). ASO-5 gapmer design and synthesis were previously described.

Surgical Delivery of Antisense Oligonucleotides

Premanifest mice used in this study received a post-natal day 0 injection of either ASO-5 or PBS into both lateral ventricles as described previously[39]. Pups were placed on ice for cryo-anesthetization before performing a bi-lateral intracerebroventricular (ICV) injection of either ASO-5 or PBS (2 µL per hemisphere, 5 µg/µL ASO-5)[39]. Pups were placed on a heating pad before returning to their cage. Pups were monitored and weighed weekly following treatment. Mice were harvested at 4 weeks of age for biochemical and histological assessment as previously described[9,40]. Symptomatic ASO treatment was completed as previously described[9,40]. Post-operative care was performed for at least 7 days following treatment.

RNA Isolation and Sequencing.

RNA was extracted from PBS-perfused, flash-frozen brainstem, spinal cord, and cerebellum samples from the left hemisphere. Using the Next Advance Bullet Blender, samples were homogenized in radioimmunoprecipitation assay (RIPA, by Sigma, St. Louis, MO) buffer (750 µL for brainstem and 500 µL for cerebellum) with added proteinase inhibitor (BioRad, Hercules, CA). A 250 µL aliquot of this lysate was reserved for Western blot analysis and the remaining sample was used for RNA extraction. RNA extraction was conducted using the QIAshredder (Qiagen Hilden, Germany), RNeasy Mini Kit (Qiagen, Hilden, Germany), and DNAse I kit (Qiagen, Hilden, Germany), then eluted in RNase-free water, according to manufacturer's instructions. RNA samples were assessed by nanodrop to determine concentration and sample purity. For library preparation, 1 µg of total brainstem and cerebellar RNA was submitted to the University of Michigan Sequencing Core for Illumina HiSeq library preparation, quality control, and RNA sequencing. We chose WT and Q84 RNA samples for RNA sequencing based on RIN number (>7 RIN) and, if applicable, CAG repeat expansion size (>average 72Q) as determined by Laragen, Inc. (Culver City, CA).

RNA-seq Expression Analyses.

The University of Michigan Bioinformatics Core generated libraries (Illumina TruSeq) from purified brain RNA samples, completed quality control analysis, and ran 75x75 paired end sequencing on Illumina HiSeq 4000. The RNAseq data were processed as previously described[21]. Briefly, reads were pseudo-aligned to the ENSEMBL 94 mouse reference cDNA sequences (Oct 2018, GRCm38p6) using Kallisto 0.45 and quantified transcripts aggregated by their gene were fed to Sleuth 0.30 for differential expression analysis. Genes with expression levels less than 5 transcripts per million (TPM) in more than 25% of the analyzed samples were discarded from the differential expression analysis. We used Sleuth to evaluate statistical significance of the differential gene expression in each of the three treatment groups: WT vehicle treated, Q84 vehicle treated, and Q84 ASO-5 treated. Through Benjamini-Hochberg correction, genes with q-values less than 0.05 were defined as differentially expressed. Gene ontology (GO)

term analysis was performed comparing the biological processes that are impaired in SCA3 compared to WT mice and that are resolved with ASO treatment in disease mice.

QPCR.

Quantitative PCR (qPCR) analysis was performed to validate the RNAseq results by reverse transcribing 0.5-1 µg of total RNA using the iScript cDNA synthesis kit according to the manufacturer's instructions (Bio-Rad, Hercules, CA). iQ quantitative PCR was performed on the diluted cDNA following the manufacturer's protocol (Bio-Rad, Hercules, CA) using the following primers: human ATXN3 (Forward primer: CCTCAATTGCACATCAGCTGGAT; Reverse primer: AACGTGCGATAATCTTCACTAGTAACTC; Probe Seq: CTGCCATTCTCATCCTC), mouse *Atxn3* (Thermofisher; Cat # Mm01336273), *Beta Actin* (Thermofisher; Cat # Mm02619580), *Smoc1* (Thermofisher; Cat #Mm00491564), *Plp1* (Thermofisher; Cat #Mm01297210), *Ugt8a* (Thermofisher; Cat #Mm00495930), *Mobp* (Thermofisher; Cat #Mm02745649), and *Mal* (Thermofisher; Cat #Mm01339780). Gene expression fold change (RQ) was calculated relative to vehicle-treated Q84 samples for each timepoint and normalized to *beta actin*, where RQ = 2-(ddCT).

Open Field Motor Evaluation

Motor assessments of Q84 mice were conducted when mice were 4 weeks old. A photobeam open-field apparatus (San Diego Instruments, San Diego, CA) was used in order to measure total locomotor activity (x/y-axis beam breaks), and exploratory behavior (z-axis beam breaks). Trials lasted for 30 minutes. Experimenters were blinded to genotypes and treatment groups during behavioral tests.

Western Blot.

Following brainstem, cerebellum, and spinal cord macrodissection, protein lysates were processed as previously described[9] and stored at -80C. Briefly, homogenized lysates were diluted, and 20-30 µg of total lysates were resolved in 4-20% gradient sodium dodecyl sulfate-polyacrylamide electrophoresis gels. Protein was transferred to 0.45 µm nitrocellulose membranes prior to overnight incubation at 4°C with the following primary

antibodies: mouse anti-ATXN3 (1H9; 1:1000, MAB5360; Millipore, Billerica, MA), mouse anti-GAPDH (1:10000, MAB374; Millipore, Billerica, MA), and rabbit anti-MOBP (1:100-1:1000; ab91405; Abcam). Following incubation, Molecular weight bands were visualized by peroxidase-conjugated anti-mouse or anti-rabbit secondary antibody (1:5000; Jackson ImmunoResearch Laboratories, West Grove, PA). ECL-plus (Western Lighting; PerkinElmer, Waltham, MA) treated membranes were visualized via exposure on G:Box Chemi XRQ system (Syngene) and band intensities were quantified using ImageJ analysis software (NIH).

Immunohistochemistry

The PBS-perfused right brain hemispheres were post-fixed for 24 hours in 4% paraformaldehyde (PFA) then sucrose-embedded. Prepared brains were sectioned and stained as previously reported[21]. Briefly, sections were washed in PBS, blocked using reagents from M.O.M. kits according to manufacturer's protocol (BMK2202, Vector Laboratories, Newark, CA), and incubated in primary antibody at 4°C overnight. Primary antibodies assessed include rabbit anti-ASO (1:5000; Ionis Pharmaceuticals, Carlsbad, CA). The following day sectioned were washed, incubated in secondary antibody and DAPI (Sigma, St. Louis, MO), washed, and mounted with Prolong Gold Antifade Reagent (Invitrogen, Waltham, MA). Fluorescent secondary antibodies used include Alexa Fluor 488 goat anti-rabbit IgG (1:1000; A11008; Invitrogen) and Alexa Fluor 647 goat anti-rabbit (1:1000; A21245; Invitrogen). Imaging was performed using a Nikon-A1 confocal microscope in peripheral tissue including the kidney, lung, and liver, as well as various brain regions, including the cortex, basilar pontine nuclei (denoted as pons), hippocampus, deep cerebellar nuclei (DCN), striatum, and cerebellar lobules.

Transmission Electron Microscopy.

Mice (1-2 males and 2 females per treatment group per region) were transcardially perfused first with 1x PBS, then with 2.5% glutaraldehyde and 4% PFA in 1x PBS. Brains were removed and postfixed overnight at 4°C in the same buffer before being transferred to 0.1M phosphate buffer, pH 7.4 for long term storage at 4°C. Processing of TEM tissue was done by University of Michigan's Microscopy Core according to their

protocol and as previously described[21]. Imaging was completed on a JEOL JEM-1400 plus transmission electron microscope (JEOL USA Inc., Peabody, MA) at an accelerating voltage of 60 kV, using either an AMT 4-megapixel XR401 or a 12-megapixel Nanosprint CMOS camera (Advanced Microscopy Techniques, Woburn, MA). For g-ratio, axon caliber, and cumulative fraction analysis of myelinated axons, MyelTracer software was used[41]. Manual counts of degenerated axons were taken as a percentage of the number of total axons used in g-ratio and axon caliber analysis per image. Experimenters were blinded to genotypes and treatment groups during TEM image analysis.

Statistics

Prism 8.0 (GraphPad Software, La Jolla, CA) was used to perform all statistical analysis. All statistical significance was evaluated using either a student's t-test or a one-way ANOVA with a post hoc Tukey's multiple comparisons test. Variability about the mean is expressed as mean ± standard error of the mean (SEM). All tests set the level of significance at $p<0.05$.

Acknowledgements:

This work was supported in part by National Ataxia Foundation SCA Young Investigator Award to H.S.M.; National Institutes of Health Grant R01-NS122751 to H.S.M., Grant T32-NS007222-33 to H.S.M., and Grant U01-NS106670 to H.S.M. We acknowledge Ionis Pharmaceuticals, who identified and generated the anti-*ATXN3* ASOs used this study. We acknowledge S. Meshinchi and D. Leroux in the Michigan Medicine Microscopy Core for TEM training and processing of TEM samples. Figure schematics were created using BioRender.com.

Author contributions:

K.H.S., A.J.Z., H.Z., Y.G., and H.S.M. designed research; K.H.S., A.J.Z., D.M.D., A.F.P., N.R.S., S.J., and H.S.M. performed research; K.H.S., A.J.Z., H.Z., D.M.D., A.F.P., N.R.S., S.J., A.N., Z.H., Y.G., and H.S.M. analyzed data; K.H.S., A.J.Z., D.M.D., A.F.P., N.R.S., H.Z., Y.G., and H.S.M. edited the paper; K.H.S., A.F.P., and H.S.M.

wrote the paper; K.H.S., A.F.P., and H.S.M. wrote the first draft of the paper; H.S.M. contributed unpublished reagents/analytic tools.

Figure Legends:

Figure 1. Neonate anti-*ATXN3* ASO injection rescues both weight and motor activity despite concentrated delivery in CNS tissue. **(A)** Illustration of neonate intracerebroventricular (ICV) injections. **(B)** Schematic of longitudinal pre-symptomatic study design. Q84 and WT mice were injected with either 20 µg of ASO-5 or vehicle treatment at post-natal day 0. Weights were recorded at 0, 1, 2, and 4 weeks of age. Open field assessment was performed prior to tissue collections at 4 weeks. **(C)** Longitudinal female and male weights from each of the 3 treatment groups. By 4-weeks-old, the weights of both male and female Q84 ASO-5 treated mice were similar to WT weights, while Q84-vehicle treated mice were significantly smaller than both other treatment groups. Open field assessment measuring **(D)** total number of X-Y beam breaks and **(E)** rearing activity of WT vehicle, Q84 vehicle, and Q84 ASO-5 treated mice at 4 weeks of age. Q84 vehicle treated mice were significantly less active than ASO-5 treated Q84 and vehicle treated WT mice, with ASO-5 treatment preventing the onset of motor and exploratory behavioral impairment at 4 weeks of age. **(F)** Representative sagittal sections of ASO-5 immunofluorescence (green) of 4-week-old ASO-5 treated SCA3 mouse brain and peripheral tissues, co-stained with DAPI (blue). ASO-5 effectively targets the whole brain, without immunofluorescence detection in peripheral tissues. Scale bar 100 µm. DCN = deep cerebellar nuclei. **(C-E)** Data (mean ± SEM) are reported (n=5-20 mice per group). One-way ANOVA with a Tukey's post hoc analysis was performed (ns=not significant, *$p<0.05$, **$p<0.01$, ****$p<0.0001$).

Figure 2. Anti-*ATXN3* ASO injections in a pre-symptomatic SCA3 mice reduce ATXN3 levels and rescue OL maturation transcriptional impairments. Quantification of **(A)** human mutant *ATXN3* and **(B)** endogenous mouse *Atxn3* transcript expression in the brainstem (BS), cerebellum (CB), and cervical spinal cord (SC) in 4-week-old treated mice. ASO-5 treatment reduced human mutant *ATXN3* and endogenous mouse *Atxn3* in both brainstem and spinal cord tissue. **(C)** Representative

western blot of high molecular weight ATXN3 species (HMW ATXN3), mutant ATXN3 (mutATXN3) and endogenous ATXN3 (endATXN3) protein expression across tissue types at 4 weeks of age. Quantification of **(D)** mutATXN3 and **(E)** HMW ATXN3 protein expression in the brainstem, cerebellum, and cervical spinal cord in treated mice. Q84 ASO-5 treatment relative to Q84 vehicle results in a reduction of HMW ATXN3 in all brain regions assessed. **(F)** Schematic of OL transcripts and corresponding maturation state. OL maturation transcript levels in the **(G)** brainstem, **(H)** cerebellum, and **(I)** cervical spinal cord in 4-week-old treated mice. OPC transcript *Smoc1* is increased in diseased spinal cord, while mature OL transcripts (*Plp1*, *Mobp*, *Ugt8a*, and *Mal1*) are decreased in all tissues assessed. Dysregulation of the majority of OPC and mature OL transcript was prevented with ASO-5 treatment in all brain regions assessed. Data (mean ± SEM) are reported relative to Q84 vehicle samples (n=3-6 mice per group). One-way ANOVA with a Tukey's post hoc analysis was performed (*p<0.05, **p<0.01, ***p<0.001, ****p<0.0001).

Figure 3. Anti-*ATXN3* ASO injections in a symptomatic SCA3 mouse reduce ATXN3 levels and rescue myelination pathways. (A) Overview of ASO treatment in 8-week-old SCA3 mice, isolation of vulnerable brain regions at 16 weeks of age, and transcriptional analysis of samples. Confirmation of the targeted partial knockdown of human ATXN3 by ASO gene silencing in **(B-E)** brainstem and **(F-I)** cerebellum. Q84 ASO treated samples compared to Q84 samples treated with vehicle. RNA-sequencing analysis of human ATXN3 disease gene expression (transcripts per million) in the brainstem **(B)** and cerebellum **(F)**. Representative western blot of disease-causing and endogenous ATXN3 in the brainstem **(C)** and cerebellum **(G)** with corresponding analysis of high molecular weight **(D, H)** and mutant ATXN3 **(E, I)**, respectively. **(J)** Heatmaps of differentially expressed WT vs Q84 vehicle treated samples from **(top)** brainstem and **(bottom)** cerebellum. **(K-L)** GO term analysis highlighting significant biological process between **(K)** WT and Q84 vehicle treated mice and **(L)** ASO-5 treated Q84 and vehicle treated Q84 mice in brainstem samples define dysfunction in myelination cholesterol biosynthesis. Data (mean ± SEM) are reported relative to Q84 vehicle samples. n=4-5 mice per group for all experiments. One-way ANOVA with a

Tukey's post hoc analysis was performed (ns=not significant, *p<0.05, **p<0.01, ***p<0.001, ****p<0.0001).

Figure 4. OL maturation pathway impairment is rescued in brainstem, cerebellar, and cervical spinal cord tissue with post-symptomatic ASO-5 treatment. OL maturation transcript levels in the **(A)** brainstem, **(B)** cerebellum, and **(C)** cervical spinal cord in 16-week-old mice treated 8 weeks earlier. OPC transcript *Smoc1* is increased in disease, while differentiating and mature OL transcripts (*Plp1, Ugt8a, Mobp,* and *Mal)* are decreased. The majority of transcript levels are rescued to WT levels with ASO-5 treatment in all brain regions assessed. Total protein levels of mature OL marker MOBP in the **(D)** brainstem, **(E)** cerebellum, and **(F)** cervical spinal cord. MOBP is decreased in disease brainstem and spinal cord and rescued with ASO-5 treatment. Data (mean ± SEM) are reported relative to Q84/Q84 vehicle samples (n=3-6 mice per group). Representative sagittal **(G)** pons and **(H)** DCN images of WT and Q84 SCA3;*MOBP*-eGFP+ mice injected with ASO-5 or vehicle at 8 weeks and collected 4 weeks later. Scale bar 50 µm. *MOBP*-eGFP+ cells are reduced in Q84 vehicle treated mice and return to vehicle-treated WT levels in disease mice treated with ASO-5. One-way ANOVA with a Tukey's post hoc analysis was performed (*p<0.05, **p<0.01, ***p<0.001).

Figure 5. Anti-*ATXN3* ASO treatment rescues myelination in the corticospinal tract and leads to hyper-myelination in the corpus callosum. (A) Representative coronal corticospinal tract (CST) TEM images depict abnormal myelination in 16-week-old Q84 vehicle treated mice that is rescued with ASO-5 injection 8 weeks prior. Scale bar, 1 µm. **(B)** Quantification of degenerated axons in the CST show no differences between treatment groups. **(C)** Analysis of CST g-ratio indicates ASO-5 treatment rescues myelin sheath thickness to WT levels. **(D)** Analysis of CST axonal caliber shows axons in Q84 ASO-5 treated mice are significantly larger relative to Q84 vehicle treated mice, but not different from WT vehicle treated mice. **(E)** Consistency of myelination across axon size is rescued with ASO-5 treatment. **(F)** Representative sagittal corpus callosum (CC) TEM images. **(G)** G-ratio analyses of CC fibers reveal significantly increased myelin sheath after ASO-5 treatment in Q84 mice, while no

changes are seen between Q84 and WT vehicle treated mice. **(H)** Axon diameter is unchanged between all treatment groups. **(I)** ASO-5 treatment affects the relationship between axon caliber and myelin thickness compared to vehicle treated mice. Axon caliber and g-ratio calculated using MyelTracer software (n=850-1250 axons across 10-15 images per mouse, n=3-4 mice per genotype). Data report as mean ± SEM. One-way ANOVA with a Tukey's post hoc analysis was performed (ns=not significant, *$p < 0.05$, **$p < 0.01$, ****$p < 0.0001$).

References

1 Costa Mdo, C. & Paulson, H. L. Toward understanding Machado-Joseph disease. *Progress in neurobiology* **97**, 239-257, doi:10.1016/j.pneurobio.2011.11.006 (2012).

2 Seidel, K. *et al.* Brain pathology of spinocerebellar ataxias. *Acta Neuropathol* **124**, 1-21, doi:10.1007/s00401-012-1000-x (2012).

3 Rub, U. *et al.* Clinical features, neurogenetics and neuropathology of the polyglutamine spinocerebellar ataxias type 1, 2, 3, 6 and 7. *Progress in neurobiology* **104**, 38-66, doi:10.1016/j.pneurobio.2013.01.001 (2013).

4 Paulson, H. L., Shakkottai, V. G., Clark, H. B. & Orr, H. T. Polyglutamine spinocerebellar ataxias - from genes to potential treatments. *Nat Rev Neurosci* **18**, 613-626, doi:10.1038/nrn.2017.92 (2017).

5 Durr, A. Autosomal dominant cerebellar ataxias: Polyglutamine expansions and beyond. *The Lancet Neurology* **9**, 885-894, doi:10.1016/S1474-4422(10)70183-6 (2010).

6 Gardiner, S. L. *et al.* Prevalence of Carriers of Intermediate and Pathological Polyglutamine Disease-Associated Alleles Among Large Population-Based Cohorts. *JAMA Neurol*, doi:10.1001/jamaneurol.2019.0423 (2019).

7 McLoughlin, H. S., Moore, L. R. & Paulson, H. L. Pathogenesis of SCA3 and implications for other polyglutamine diseases. *Neurobiol Dis* **134**, 104635, doi:10.1016/j.nbd.2019.104635 (2020).

8 Schmitt, I. *et al.* Inactivation of the mouse Atxn3 (ataxin-3) gene increases protein ubiquitination. *Biochem Biophys Res Commun* **362**, 734-739, doi:10.1016/j.bbrc.2007.08.062 (2007).

9 Moore, L. R. *et al.* Evaluation of Antisense Oligonucleotides Targeting ATXN3 in SCA3 Mouse Models. *Mol Ther Nucleic Acids* **7**, 200-210, doi:10.1016/j.omtn.2017.04.005 (2017).

10 Moore, L. R. *et al.* Antisense oligonucleotide therapy rescues aggresome formation in a novel spinocerebellar ataxia type 3 human embryonic stem cell line. *Stem Cell Res* **39**, 101504, doi:10.1016/j.scr.2019.101504 (2019).

11 Reina, C. P., Nabet, B. Y., Young, P. D. & Pittman, R. N. Basal and stress-induced Hsp70 are modulated by ataxin-3. *Cell Stress Chaperones* **17**, 729-742, doi:10.1007/s12192-012-0346-2 (2012).

12 Chiriboga, C. A. *et al.* Results from a phase 1 study of nusinersen (ISIS-SMN(Rx)) in children with spinal muscular atrophy. *Neurology* **86**, 890-897, doi:10.1212/WNL.0000000000002445 (2016).

13 Bennett, C. F. & Swayze, E. E. RNA targeting therapeutics: molecular mechanisms of antisense oligonucleotides as a therapeutic platform. *Annu Rev Pharmacol Toxicol* **50**, 259-293, doi:10.1146/annurev.pharmtox.010909.105654 (2010).

14 Yu, R. Z. *et al.* Tissue disposition of 2'-O-(2-methoxy) ethyl modified antisense oligonucleotides in monkeys. *J Pharm Sci* **93**, 48-59, doi:10.1002/jps.10473 (2004).

15 Finkel, R. S. *et al.* Treatment of infantile-onset spinal muscular atrophy with nusinersen: a phase 2, open-label, dose-escalation study. *Lancet* **388**, 3017-3026, doi:10.1016/S0140-6736(16)31408-8 (2016).

16 Finkel, R. S. *et al.* Nusinersen versus Sham Control in Infantile-Onset Spinal Muscular Atrophy. *N Engl J Med* **377**, 1723-1732, doi:10.1056/NEJMoa1702752 (2017).

17 Bushart, D. D. *et al.* Antisense Oligonucleotide Therapy Targeted Against ATXN3 Improves Potassium Channel-Mediated Purkinje Neuron Dysfunction in Spinocerebellar Ataxia Type 3. *Cerebellum*, doi:10.1007/s12311-020-01179-7 (2020).

18 McLoughlin, H. S. *et al.* Oligonucleotide therapy mitigates disease in spinocerebellar ataxia type 3 mice. *Ann Neurol* **84**, 64-77, doi:10.1002/ana.25264 (2018).

19 Toonen, L. J., Schmidt, I., Luijsterburg, M. S., van Attikum, H. & van Roon-Mom, W. M. Antisense oligonucleotide-mediated exon skipping as a strategy to reduce proteolytic cleavage of ataxin-3. *Sci Rep* **6**, 35200, doi:10.1038/srep35200 (2016).

20 Toonen, L. J. A., Rigo, F., van Attikum, H. & van Roon-Mom, W. M. C. Antisense Oligonucleotide-Mediated Removal of the Polyglutamine Repeat in Spinocerebellar Ataxia Type 3 Mice. *Mol Ther Nucleic Acids* **8**, 232-242, doi:10.1016/j.omtn.2017.06.019 (2017).

21 Schuster, K. H. *et al.* Impaired oligodendrocyte maturation is an early feature in SCA3 disease pathogenesis. *Journal of Neuroscience* **42**, doi:10.1523/Jneurosci.1954-20.2021 (2022).

22 Costa, M. D. C. *et al.* In Vivo Molecular Signatures of Cerebellar Pathology in Spinocerebellar Ataxia Type 3. *Mov Disord*, doi:10.1002/mds.28140 (2020).

23 Kenigsbuch, M. *et al.* A shared disease-associated oligodendrocyte signature among multiple CNS pathologies. *Nat Neurosci*, doi:10.1038/s41593-022-01104-7 (2022).

24 Ferrari Bardile, C. *et al.* Intrinsic mutant HTT-mediated defects in oligodendroglia cause myelination deficits and behavioral abnormalities in Huntington disease. *Proc Natl Acad Sci U S A* **116**, 9622-9627, doi:10.1073/pnas.1818042116 (2019).

25 Philips, T. *et al.* Oligodendrocyte dysfunction in the pathogenesis of amyotrophic lateral sclerosis. *Brain* **136**, 471-482, doi:10.1093/brain/aws339 (2013).

26 Errea, O. & Rodriguez-Oroz, M. C. Oligodendrocytes, a New Player in the Etiology of Parkinson's Disease. *Mov Disord* **36**, 83, doi:10.1002/mds.28393 (2021).

27 Spitzer, S. O. *et al.* Oligodendrocyte Progenitor Cells Become Regionally Diverse and Heterogeneous with Age. *Neuron* **101**, 459-471 e455, doi:10.1016/j.neuron.2018.12.020 (2019).

28 Costa Mdo, C. *et al.* Toward RNAi therapy for the polyglutamine disease Machado-Joseph disease. *Mol Ther* **21**, 1898-1908 (2013).

29 Cemal, C. K. *et al.* YAC transgenic mice carrying pathological alleles of the MJD1 locus exhibit a mild and slowly progressive cerebellar deficit. *Hum Mol Genet* **11**, 1075-1094 (2002).

30 Gong, S. *et al.* A gene expression atlas of the central nervous system based on bacterial artificial chromosomes. *Nature* **425**, 917-925, doi:10.1038/nature02033 (2003).

31 Inada, B. S. Y. *et al.* Corticospinal tract involvement in spinocerebellar ataxia type 3: a diffusion tensor imaging study. *Neuroradiology*, doi:10.1007/s00234-020-02528-3 (2020).

32 Jafar-Nejad, P. *et al.* The atlas of RNase H antisense oligonucleotide distribution and activity in the CNS of rodents and non-human primates following central administration. *Nucleic Acids Res* **49**, 657-673, doi:10.1093/nar/gkaa1235 (2021).

33 Chauhan, N. B. Trafficking of intracerebroventricularly injected antisense oligonucleotides in the mouse brain. *Antisense Nucleic Acid Drug Dev* **12**, 353-357, doi:10.1089/108729002761381320 (2002).

34 Casaca-Carreira, J., Temel, Y., Larrakoetxea, I. & Jahanshahi, A. Distribution and Penetration of Intracerebroventricularly Administered 2'OMePS Oligonucleotide in the Mouse Brain. *Nucleic Acid Ther* **27**, 4-10, doi:10.1089/nat.2016.0642 (2017).

35 Silva, A. C. *et al.* Antisense oligonucleotide therapeutics in neurodegenerative diseases: the case of polyglutamine disorders. *Brain* **143**, 407-429, doi:10.1093/brain/awz328 (2020).

36 Siegel, G. J. *Basic neurochemistry : molecular, cellular, and medical aspects*. 6th edn, (Lippincott Williams & Wilkins, 1999).

37 Snipes, G. J. & Suter, U. Cholesterol and myelin. *Subcell Biochem* **28**, 173-204, doi:10.1007/978-1-4615-5901-6_7 (1997).

38 Johnson, S. L. *et al.* Drosophila as a Model of Unconventional Translation in Spinocerebellar Ataxia Type 3. *Cells* **11**, doi:10.3390/cells11071223 (2022).

39 Kim, J. Y., Grunke, S. D., Levites, Y., Golde, T. E. & Jankowsky, J. L. Intracerebroventricular viral injection of the neonatal mouse brain for persistent and widespread neuronal transduction. *J Vis Exp*, 51863, doi:10.3791/51863 (2014).

40 McLoughlin, H. S. *et al.* Oligonucleotide therapy mitigates disease in Spinocerebellar Ataxia Type 3 mice. *Annals of Neurology* **81**, 64-77, doi:10.1002/ana.25264 (2018).

41 Kaiser, T. *et al.* MyelTracer: A Semi-Automated Software for Myelin g-Ratio Quantification. *eNeuro* **8**, doi:10.1523/ENEURO.0558-20.2021 (2021).

Figure 1

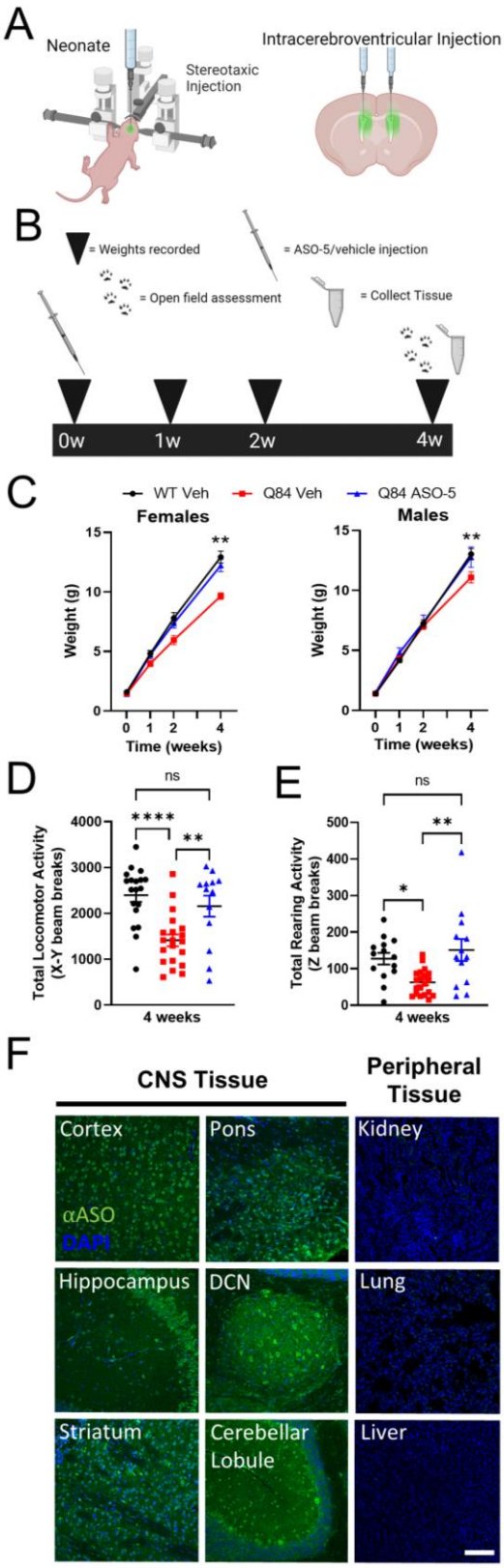
A
Neonate
Stereotaxic Injection
Intracerebroventricular Injection
B
= Weights recorded
= ASO-5/vehicle injection
= Open field assessment
= Collect Tissue
0w
1w
2w
4w
C
WT Veh
Q84 Veh
Q84 ASO-5
Females
Males
Weight (g)
Time (weeks)
D
Total Locomotor Activity (X-Y beam breaks)
4 weeks
ns
****
**
E
Total Rearing Activity (Z beam breaks)
4 weeks
ns
*
**
F
CNS Tissue
Peripheral Tissue
Cortex
αASO
DAPI
Pons
Kidney
Hippocampus
DCN
Lung
Striatum
Cerebellar Lobule
Liver

Figure 2

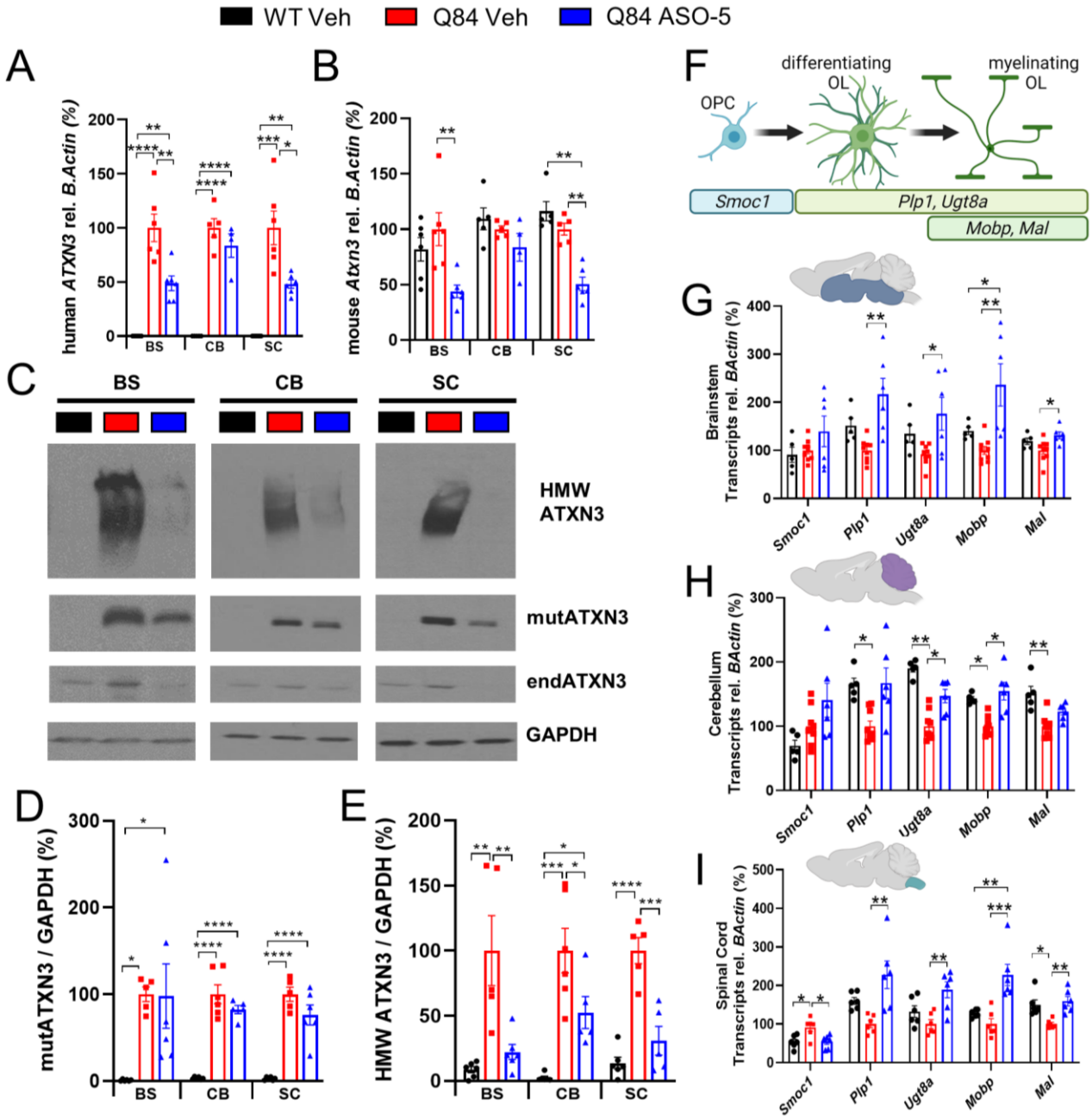
WT Veh
Q84 Veh
Q84 ASO-5
A
human ATXN3 rel. B.Actin (%)
BS
CB
SC
B
mouse Atxn3 rel. B.Actin (%)
C
HMW ATXN3
mutATXN3
endATXN3
GAPDH
D
mutATXN3 / GAPDH (%)
E
HMW ATXN3 / GAPDH (%)
F
OPC
differentiating OL
myelinating OL
Smoc1
Plp1, Ugt8a
Mobp, Mal
G
Brainstem Transcripts rel. BActin (%)
H
Cerebellum Transcripts rel. BActin (%)
I
Spinal Cord Transcripts rel. BActin (%)

Figure 3

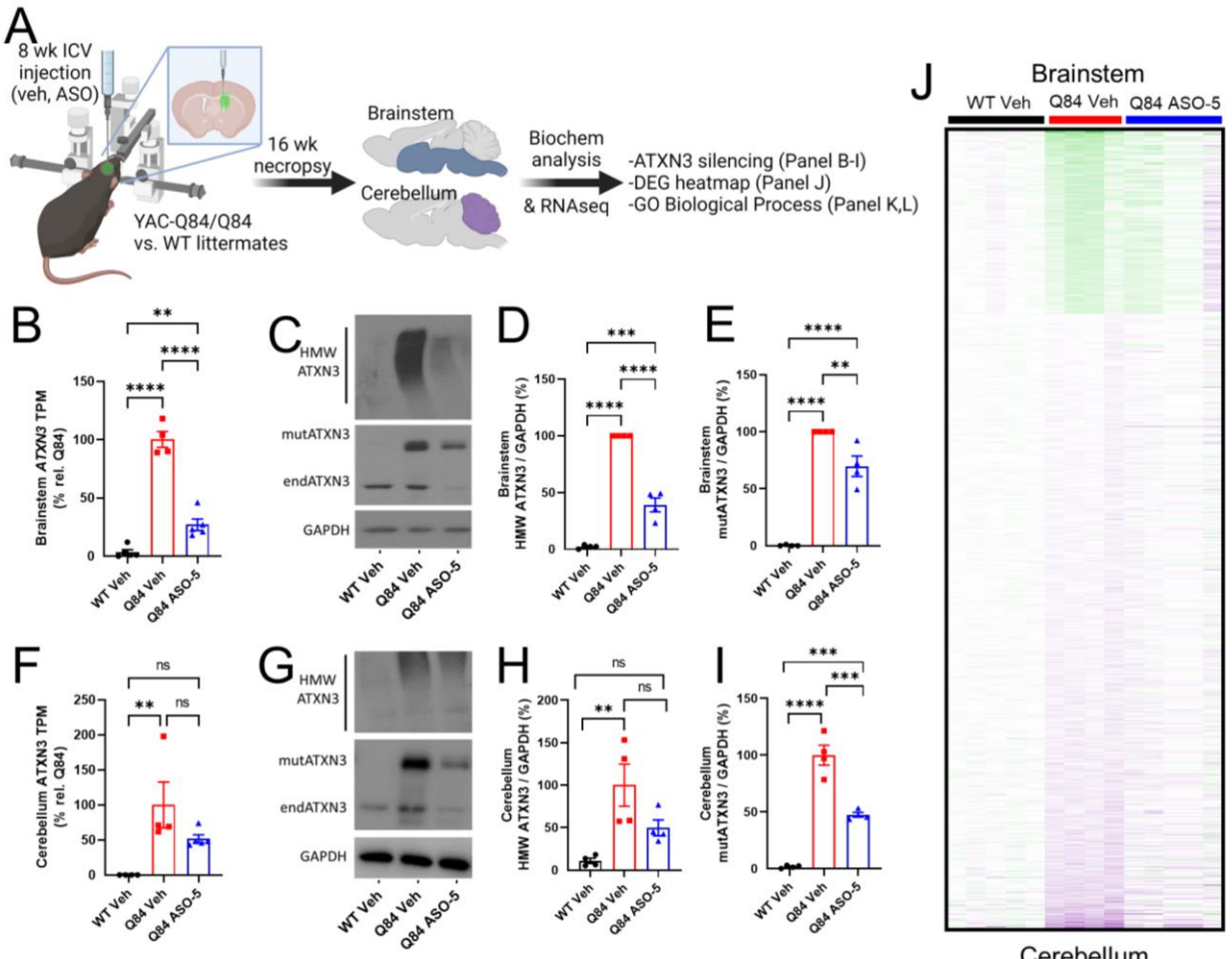

K

Gene Ontology Biological Processes (WT Veh vs. Q84 Veh)	p-value
Sterol biosynthetic process	$8.0e^{-3}$
Cholesterol biosynthetic process	$2.2e^{-2}$
Secondary alcohol biosynthetic process	$2.2e^{-2}$
Monocyte chemotactic protein-1 production	$17.2e^{-2}$
Regulation of monocyte chemotactic protein-1 production	$17.2e^{-2}$

L

Gene Ontology Biological Processes (Q84 Veh vs. Q84 ASO)	p-value
Ensheathment of neurons	$1.62e^{-4}$
Axon ensheathment	$1.62e^{-4}$
Myelination	$2.0e^{-3}$
Glial cell differentiation	$2.0e^{-3}$
Organic hydroxy compound biosynthesis process	$3.0e^{-3}$

Figure 4

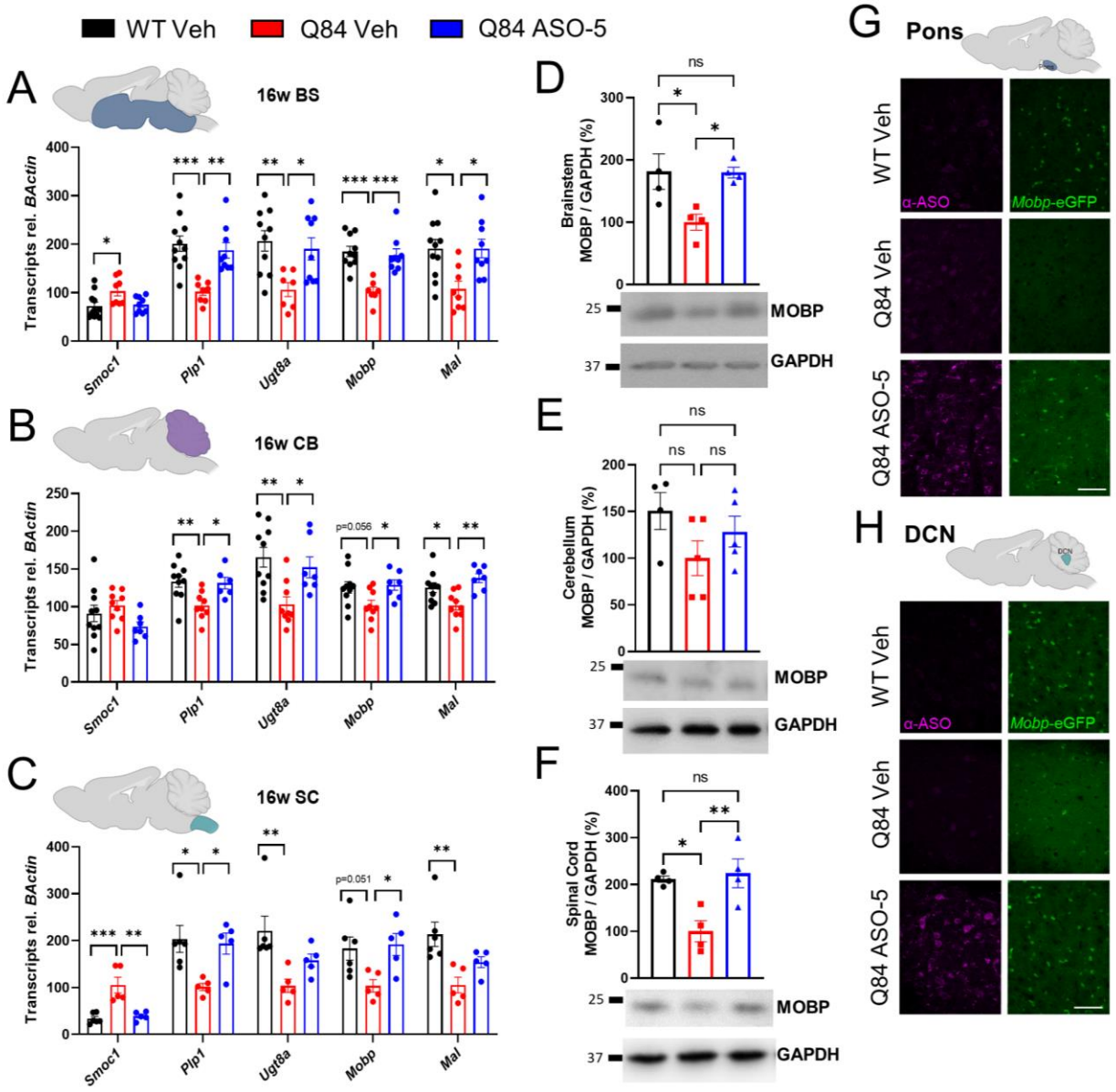
WT Veh
Q84 Veh
Q84 ASO-5
A
16w BS
B
16w CB
C
16w SC
Transcripts rel. BActin
Smoc1
Plp1
Ugt8a
Mobp
Mal
p=0.056
p=0.051
D
Brainstem
MOBP / GAPDH (%)
E
Cerebellum
MOBP / GAPDH (%)
F
Spinal Cord
MOBP / GAPDH (%)
ns
MOBP
GAPDH
G
Pons
H
DCN
α-ASO
Mobp-eGFP

Figure 5

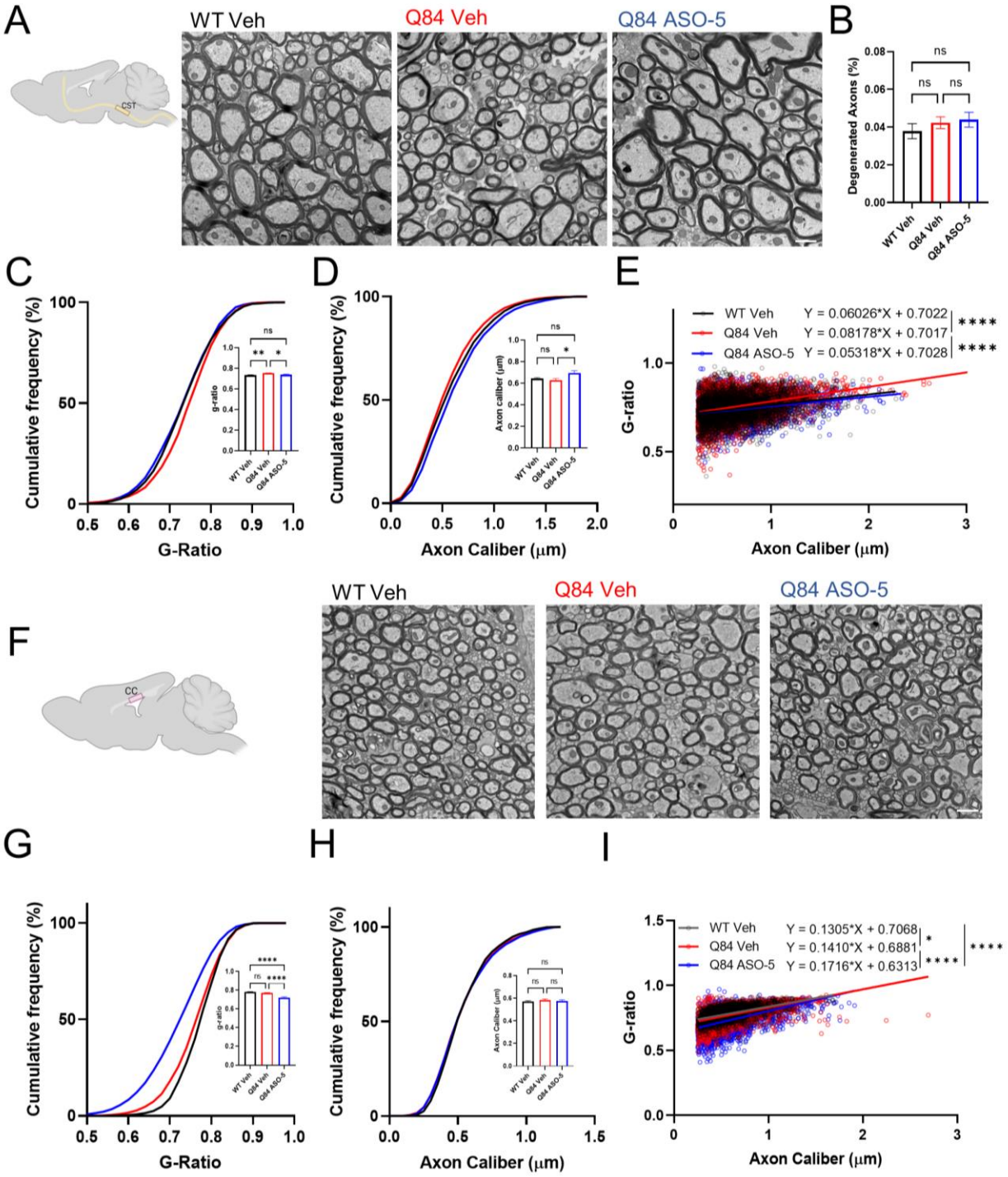
A
WT Veh
Q84 Veh
Q84 ASO-5
CST
B
Degenerated Axons (%)
ns
C
Cumulative frequency (%)
G-Ratio
g-ratio
D
Axon Caliber (μm)
E
G-ratio
WT Veh Y = 0.06026*X + 0.7022
Q84 Veh Y = 0.08178*X + 0.7017
Q84 ASO-5 Y = 0.05318*X + 0.7028
****
F
CC
G
H
I
WT Veh Y = 0.1305*X + 0.7068
Q84 Veh Y = 0.1410*X + 0.6881
Q84 ASO-5 Y = 0.1716*X + 0.6313